Electronic Supplementary Information for Dalton Transactions

Supporting Information

Enantiopure Chiral Coordination Polymers of Tetrahedral and Octahedral Cobalt(II) Alternate Chains Exhibiting Slow Magnetic Relaxation Bahavior

Dong-Rong Xiao,*[a] Guang-Ju Zhang,[a] Jun-Liang Liu,[b] Lin-Lin Fan,[b] Ruo Yuan,[a] and Ming-Liang Tong*[b]

[a] *College of Chemistry and Chemical Engineering, Southwest University, Chongqing, 400715, P. R. China. E-mail: xiaodr98@yahoo.com.cn*

[b] *Key Laboratory of Bioinorganic and Synthetic Chemistry of Ministry of Education, State Key Laboratory of Optoelectronic Materials and Technologies, School of Chemistry and Chemical Engineering, Sun Yat-Sen University, Guangzhou 510275, P. R. China.* E-mail: tongml@mail.sysu.edu.cn

I. Experimental Section

1. Materials and Measurements

All chemicals were commercially purchased and used without further purification. Elemental analyses (C, H and N) were performed on a Perkin-Elmer 2400 CHN Elemental Analyzer. The content of Co was determined by a Leaman inductively coupled plasma (ICP) spectrometer. IR spectra were recorded in the range 400-4000 cm^{-1} on an Alpha Centaurt FT/IR Spectrophotometer using KBr pellets. TG analyses were performed on a Perkin-Elmer TGA7 instrument in flowing N_2 with a heating rate of 10 ºC·min^{-1}. The circular dichroism spectra were recorded on a JASCO J−810 Spectropolarimeter with KBr pellets. Magnetic susceptibility measurements were obtained with the use of a Quantum Design MPMS-XL7 SQUID magnetometer at temperatures ranging from 1.8 to 300 K. The DC measurements were collected using applied fields in the range 0−7 T. Data were corrected for diamagnetic contributions calculated from Pascal constants. The AC measurements were performed at various frequencies from 1 to 1488 Hz with the AC field amplitude of 5 Oe and no DC field applied.

2. Experimental Details

Synthesis of D-1: A mixture of $Co(OAc)_2·4H_2O$ (0.6 mmol), H_2sdba (0.4mmol) , D-tryptophan (0.6 mmol) and water (9 mL) was stirred for 30 min in air, then transferred and sealed in an 18 mL Teflon-lined autoclave, which was heated at 130 ˚C for 4 d. After slow cooling to room temperature, purple prism crystals of **D-1** were filtered off, washed with distilled water, and dried at ambient temperature (yield: 184 mg, 74% based on Co). Elemental analysis calcd (%) for $C_{36}H_{30}Co_2N_4O_{10}S$: C 52.19, H 3.65, Co 14.23, N 6.76; found: C 51.89, H 3.47, Co 14.38, N 7.01. IR (KBr): $\tilde{\nu}$ = 3416(s), 3355(m), 3278(w), 3055(w), 2954(w), 2935(w), 2903(w), 2837(w), 1682(s),

1626(s), 1599(s), 1558(s), 1486(w), 1456(m), 1404(s), 1346(w), 1315(m), 1294(m), 1262(m), 1160(s), 1136(s), 1099(s), 1071(s), 1052(w), 1013(m), 983(w), 931(w), 905(w), 867(m), 819(w), 803(w), 775(w), 740(s), 720(w), 689(m), 626(m), 589(m), 575(w), 549(m), 504(m), 473(w), 424(m) cm^{-1}.

L-1 was prepared in a similar fashion to **D-1** except that L-tryptophan was used instead of D-tryptophan (yield: 176 mg, 71% based on Co). Elemental analysis calcd (%) for $C_{36}H_{30}Co_2N_4O_{10}S$: C 52.19, H 3.65, Co 14.23, N 6.76; found: C 51.97, H 3.78, Co 14.46, N 6.94. IR (KBr): $\tilde{\nu}$ = 3417(s), 3356(m), 3279(w), 3055(w), 2935(w), 2903(w), 1682(s), 1625(s), 1600(s), 1559(s), 1489(w), 1456(m), 1404(s), 1345(w), 1317(m), 1295(m), 1261(m), 1159(s), 1136(m), 1099(s), 1072(s), 1053(w), 1013(m), 984(w), 932(w), 905(w), 867(m), 804(w), 775(w), 741(s), 719(w), 688(m), 625(m), 589(m), 549(m), 503(m), 474(w), 424(m) cm^{-1}.

3. Synthetic discussion

In our experiments, the *L*- or *D*-tryptophan (*L*- or *D*-Trp) and long V-shaped 4,4'-sulfonyldibenzoate (sdba) ligands are simultaneously introduced based on the following considerations: (i) Recent works have indicated that the chiral amino acids are suitable ligands for the construction of coordination polymers with extended M-O-M connectivity.[1] Therefore, it should be possible to link anisotropic metal ions by the caping Trp ligands to give a 1D chiral chain with strong intrachain magnetic couplings. (ii) As a weaker magnetic mediator, sdba can double function as a structural linker and magnetic separator, which may prevent magnetic interactions between the chiral chains and thus provide a chance to obtain chiral 2D or 3D networks exhibiting SCMs behaviour.[2]

(1) (a) Anokhina, E. V.; Go, Y. B.; Lee, Y.; Vogt, T.; Jacobson, A. J. *J. Am. Chem. Soc.* **2006**, *128*,

9957. (b) Anokhina, E. V.; Jacobson, A. J. *J. Am. Chem. Soc.* **2004**, *126*, 3044.

(2) (a) Zheng, Y.-Z.; Tong, M.-L.; Zhang, W.-X.; Chen, X.-M. *Angew.Chem. Int. Ed.* **2006**, *45*, 6310. (b) Zhang, X.-M.; Hao, Z.-M.; Zhang, W.-X.; Chen, X.-M. *Angew. Chem. Int. Ed.* **2007**, *46*, 3456. (c) Hu, S.; Yun, L.; Zheng, Y.-Z.; Lan, Y.-H.; Powell, A. K.; Tong, M.-L. *Dalton Trans.* **2009**, 1897. (d) Zheng, Y.-Z.; Xue, W.; Tong, M.-L.; Chen, X.-M.; Zheng, S.-L. *Inorg. Chem.* **2008**, *47*, 11202.

4. X-ray Crystallography

Suitable single crystals with dimensions of 0.49 × 0.29 × 0.23 mm for **D-1** and 0.51 × 0.27 × 0.25 mm for **L-1** were glued on a glass fiber. Diffraction intensity data were collected on a Bruker Apex CCD diffractometer with graphite-monochromated Mo Kα radiation (λ=0.71073Å) at 293K. Absorption corrections were applied using the multiscan technique. The structures were solved by the direct method and refined by the full-matrix least-squares method on F^2 using the SHELXL-97 software.[3] All of the non-hydrogen atoms were refined anisotropically. The organic hydrogen atoms were generated geometrically. The Flack parameters of 0.014(10) and 0.014(11) for **D-1** and **L-1** indicate that the absolute configurations are correct.

(3) (a) Sheldrick, G. M. *SHELXS 97, Program for Crystal Structure Solution*; University of Göttingen: Germany, 1997; (b) Sheldrick, G. M. *SHELXL 97, Program for Crystal Structure Refinement*, University of Göttingen: Germany, 1997.

5. Discussion on magnetism

Heisenberg and Ising chain models are widely used in studying SCM behavior, but the real system is more complicated. In most cased, single-ion anisotropy and the magnetic interaction are both relevant.

As we know in the Ising model, large oriented domains of 2ξ length along the chain are separated by narrow domain walls. In this situation, the susceptibility of the chain at low temperatures is given by the following relation

$$\chi'T = C_{\text{eff}} \exp(\Delta_\xi / k_B T)$$

where Δ_ξ is the energy to create a domain wall, C is the Curie constant per magnetic unit, and k_B is the Boltzmann constant. In the presence of a very small number of defects along the chain, the correlation length (ξ) is longer than the finite chain (L), which is called finite-size effect, leading to the decrease of $\chi_m T$ below a crossover temperature, T^*. Due to the finite-size effect, when below T^*, all of the spins are parallel within the segment and can be reduced as an effective spin of nS, so each segment shows a Curie-like behavior with $n = (\chi'T)_{max}/C_{\text{eff}}$. In the Ising limit, narrow domain walls are expected with $\Delta_\xi = 4|J|S^2$.

Considering the single-ion anisotropy, D, the energy to reverse this spin is $\Delta_A = |D|S^2$.

For $T > T^*$ (~3.6 K), the dynamics is the same as that for the infinite chain, the energy gap of $\Delta_{\tau 1} = 2\Delta_\xi + \Delta_A$ ($2\Delta_\xi$ is attributed to two ends of the domain walls). For $T < T^*$, because these terminal spins are linked to only one neighbor and they have to overcome only one interaction to reverse, so $\Delta_{\tau 1} = \Delta_\xi + \Delta_A$.[4]

In our cases, the slope of $\ln(\chi'T)$ vs $1/T$ plots indicates the creation of the domain wall Δ_ξ/k_B = 20.1 K and C_{eff} = 0.27 cm^3 K mol^{-1}. Fitting by the Arrhenius law, $\Delta_{\tau 1}$ (63.7 K) and $\Delta_{\tau 2}$ (49.3 K) were obtained above and below T^*, respectively.

$$\Delta_{\tau 1} = 2\Delta_\xi + \Delta_A$$
$$\Delta_{\tau 2} = \Delta_\xi + \Delta_A$$

So, Δ_A can be calculated as ~26.4 K. And the spin units of each segment is $n = (\chi'T)_{max}/C_{\text{eff}}$, that is, ~53 units.

(4) (a) Coulon, C.; Miyasaka, H.; Clérac, R. *Struct. Bonding (Berlin)* **2006**, *122*, 163 and references therein. (b) Bogani, L.; Vindigni, A.; Sessolia, R.; Gatteschia, D. *J. Mater. Chem.* **2008**, *18*, 4750 and references therein. (c) Bogani, L.; Caneschi, A.; Fedi, M.; Gatteschi, D.; Massi, M.; Novak, M. A.; Pini, M. G.; Rettori, A.; Sessoli R.; Vindigni, A. *Phys. Rev. Lett.* **2004**, *92*, 207204. (d) Miyasaka, H.; Julve, M.; Yamashita, M.; Clérac, R. *Inorg. Chem.* **2009**, *48*, 3420 and references therein.

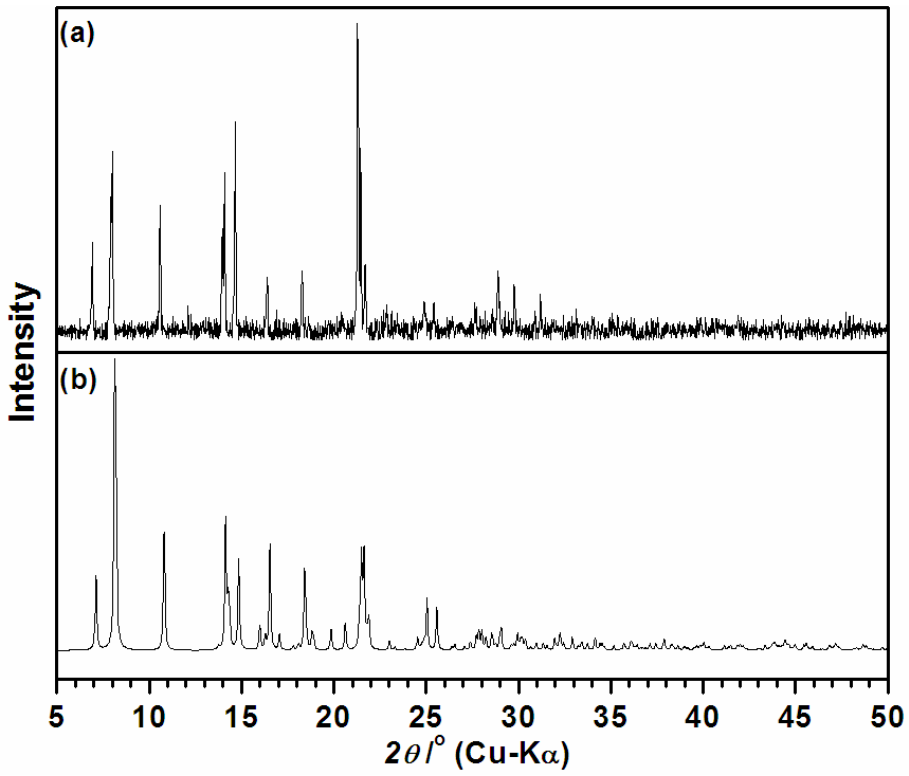

Figure S1. XRPD patterns of **D-1**: (a) experimental XRPD at room temperature; (b) simulated XRPD from single-crystal X-ray diffraction data.

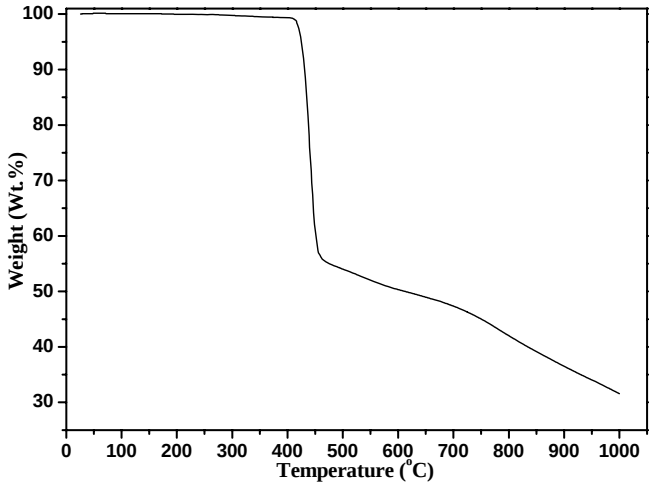

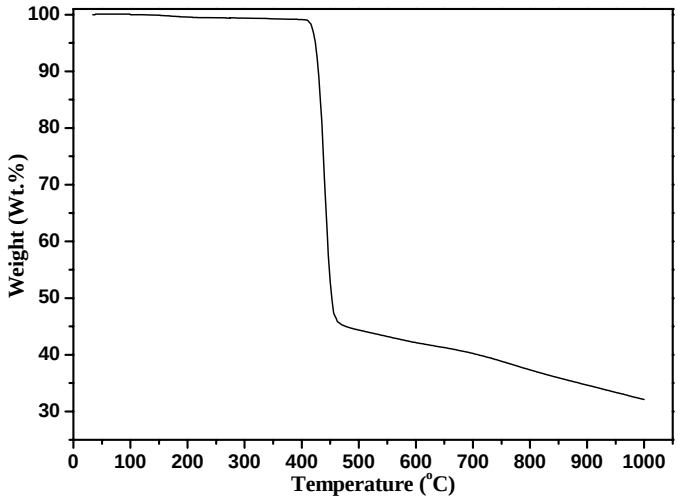

Figure S2. The TG curves of compounds **D-1** (a) and **L-1** (b) under a nitrogen atmosphere (10 °C/min).

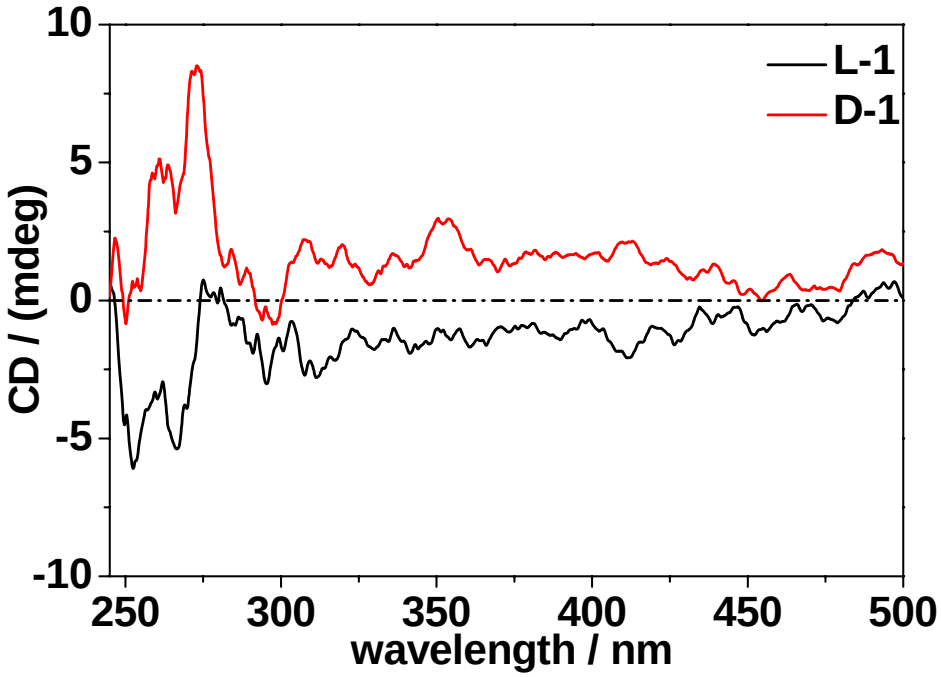

Figure S3. Solid state CD spectra of **D-1** (red) and **L-1** (black) in KBr pellets.

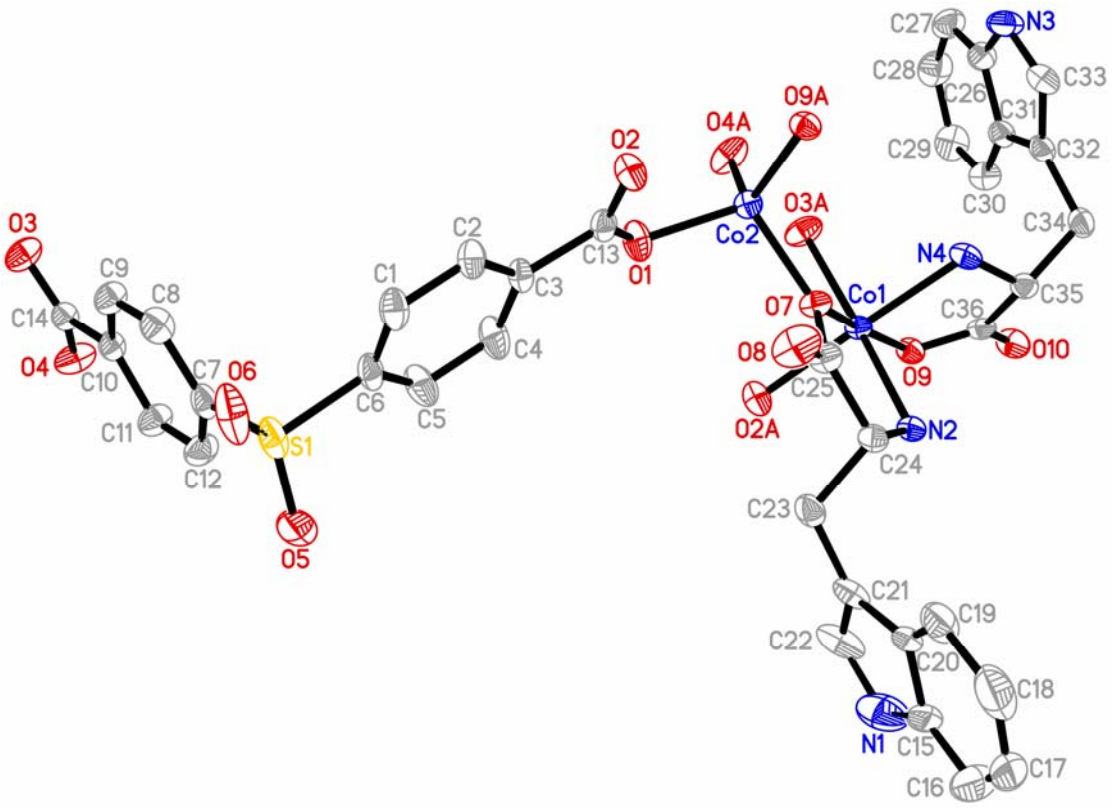

Figure S4. ORTEP drawing of the coordination geometries in **D-1** with thermal ellipsoids at 30% probability.

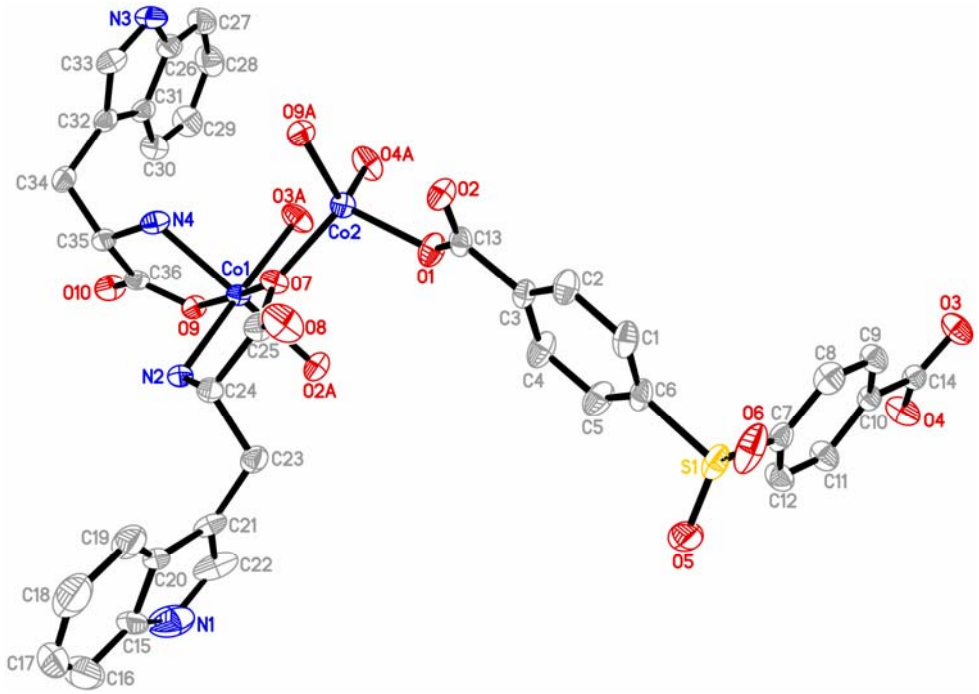

Figure S5. ORTEP drawing of the coordination geometries in **L-1** with thermal ellipsoids at 30% probability.

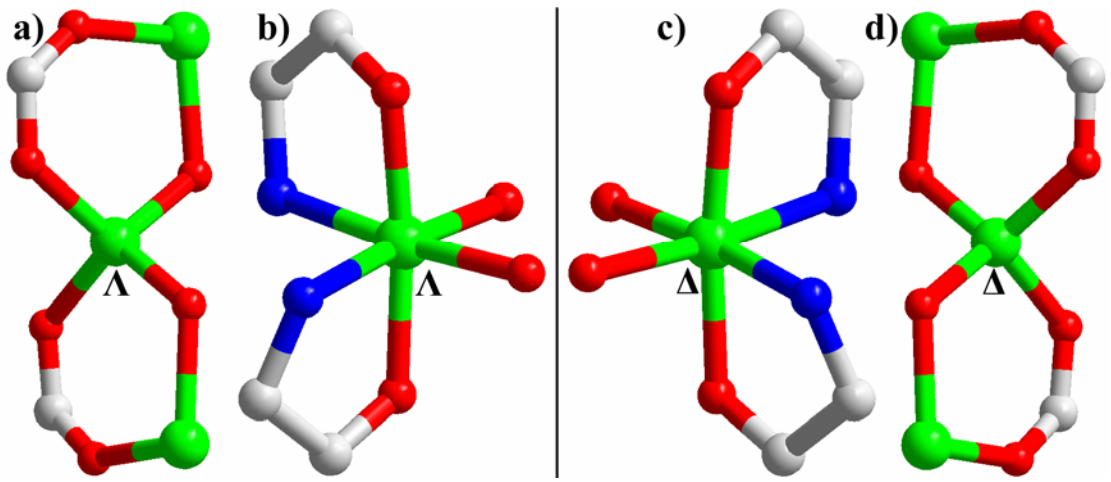

Figure S6. (a, b) Perspective views of the Λ octahedral Co1 center (b) and Λ Co2 center (a) in **D-1**. (c, d) The Δ octahedral Co1 center and Δ tetrahedral Co2 center in **L-1**.

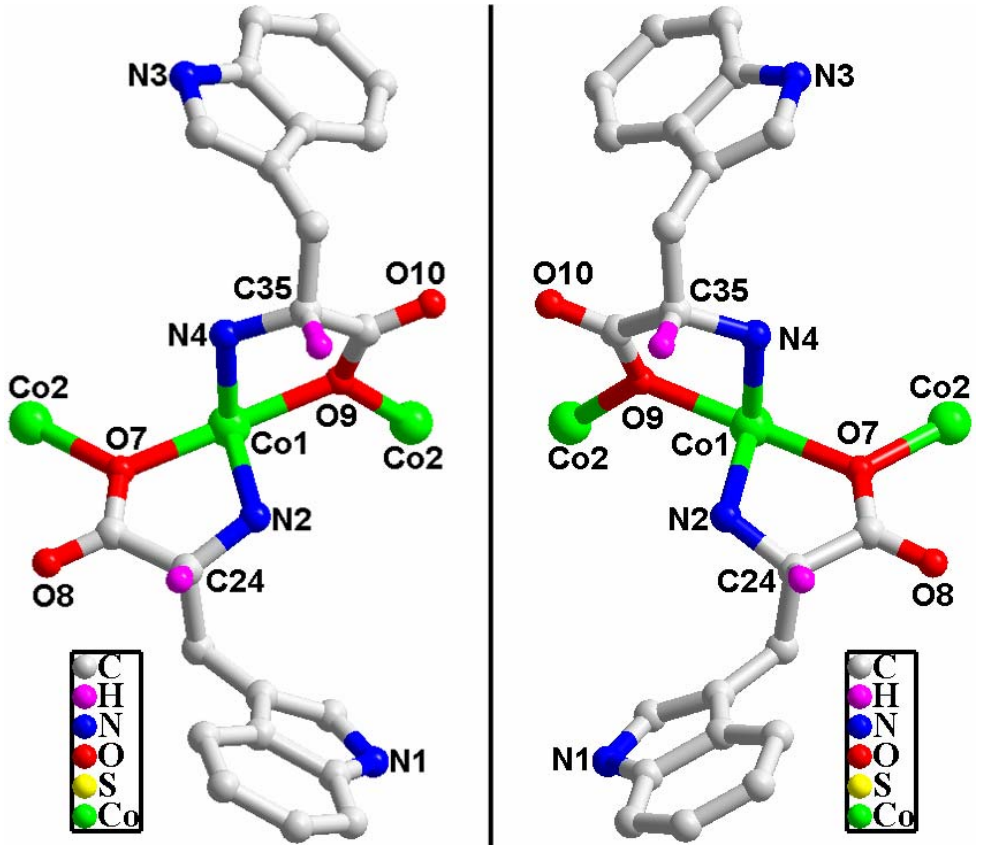

Figure S7. The coordination modes for D-Trp in **D-1** (left) and for L-Trp in **L-1** (right).

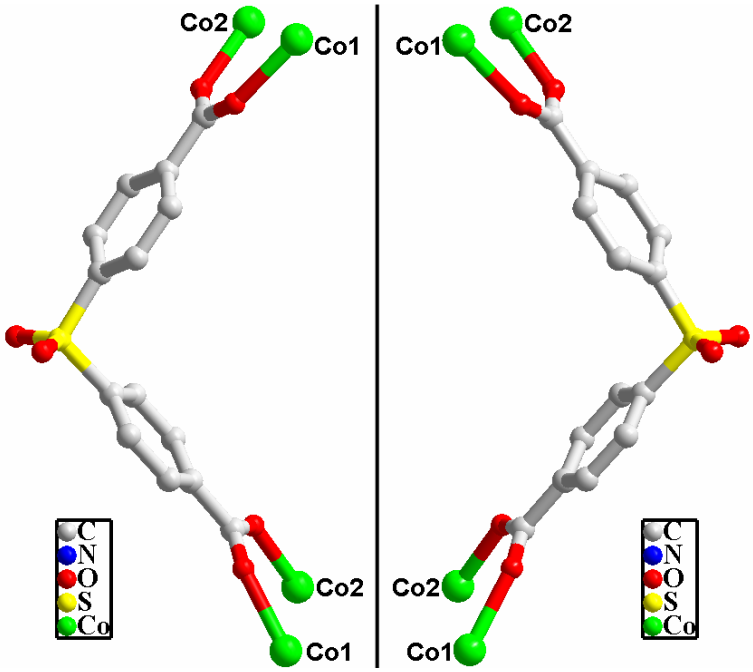

Figure S8. Coordination modes of the sdba ligand in **D-1** (left) and **L-1** (right).

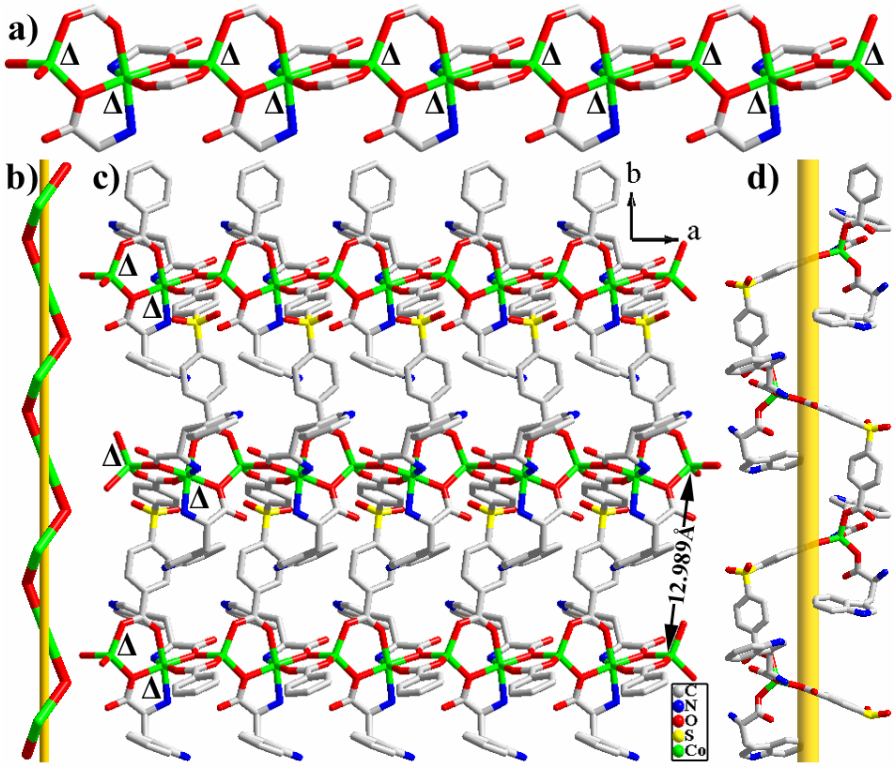

Figure S9. Perspective views of the carboxylate-bridged Co–O–Co chain (a) in the 2D chiral layer (c), highlighting two types of vertical homochiral helices (b, d) in **L-1**.

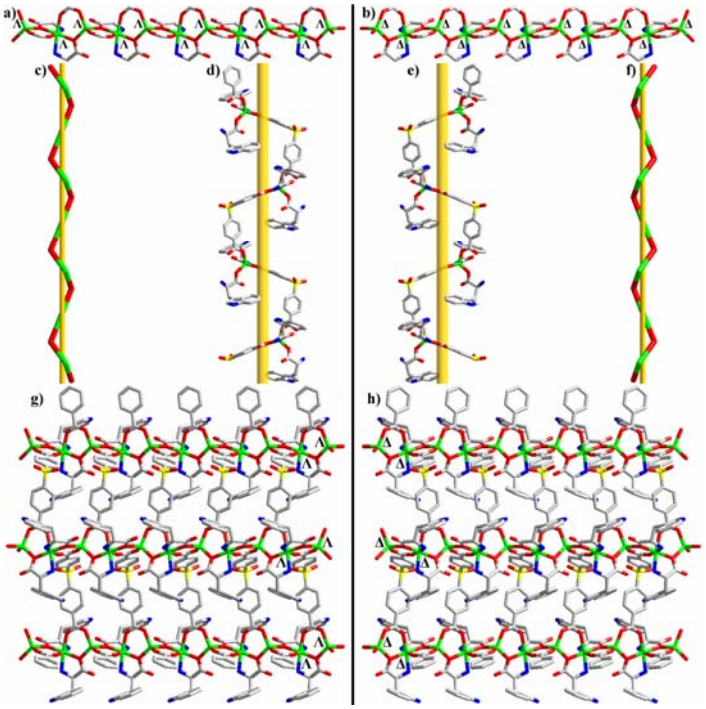

Figure S10. Crystal structures of the enantiomeric pair of **1**: **D-1** (left) and **L-1** (right). (a, b) Perspective views of the carboxylate-bridged Co–O–Co chains in **D-1** (left) and **L-1** (right). (c, d, e, f) Perspective views of two types of vertical homochiral helices in **D-1** (left) and **L-1** (right). (g, h) Perspective views of the 2D chiral layers in **D-1** (left) and **L-1** (right).

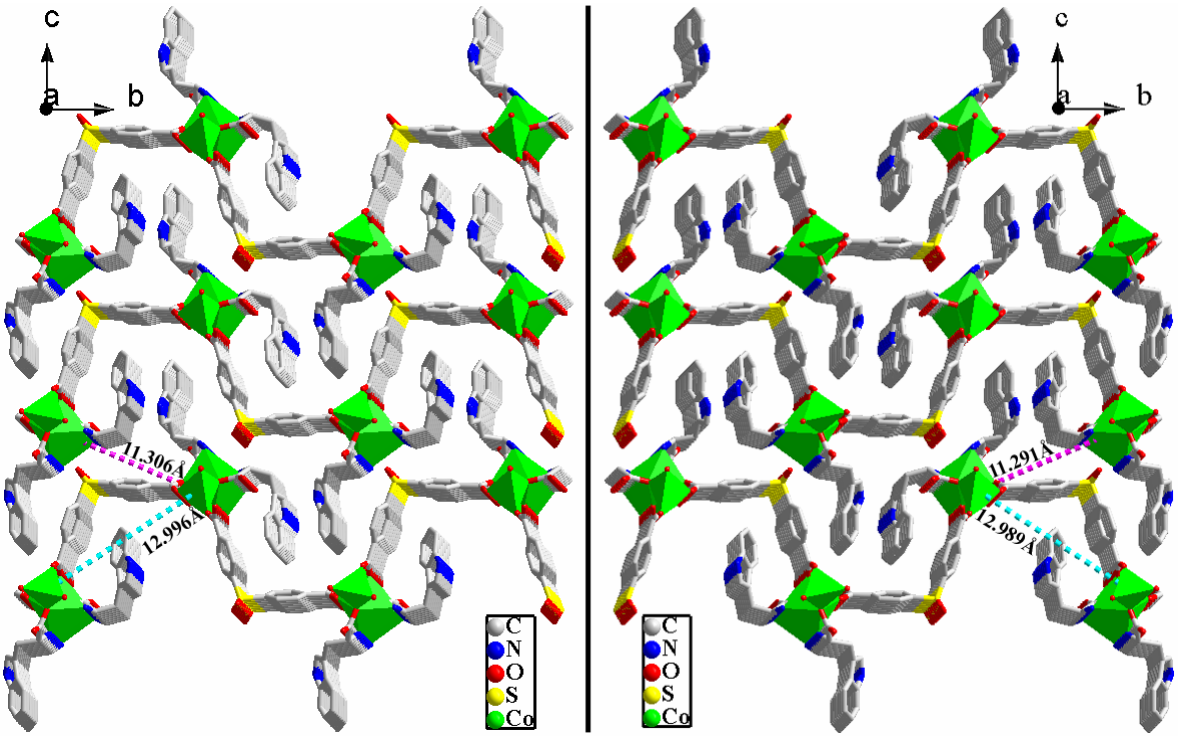

Figure S11. The chiral 3D supramolecular networks of **D-1** (left) and **L-1** (right).

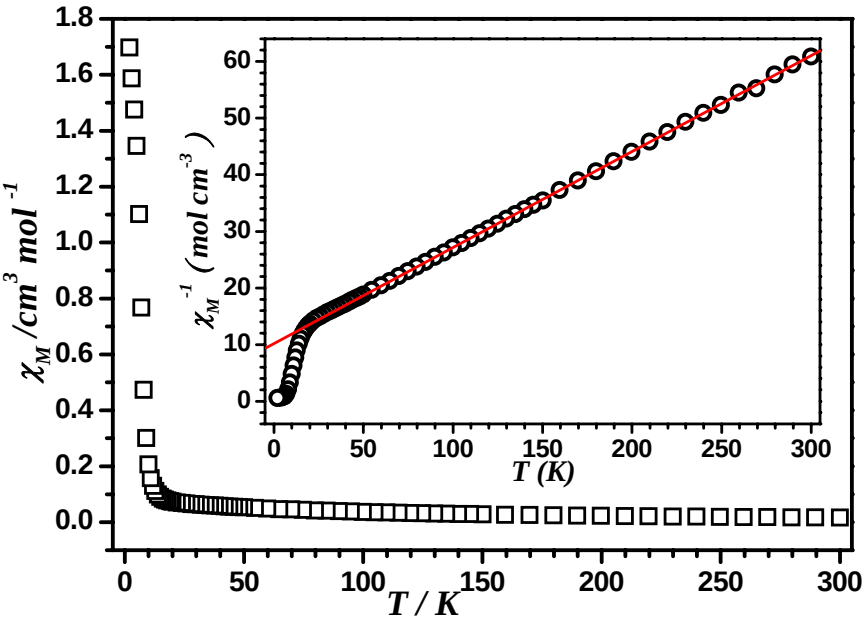

Figure S12. Temperature dependence of the magnetic susceptibility χ_M (being defined as M/H per Co_2 unit) for **L-1** under 1.0 kOe. Insert: Temperature dependence of χ_M^{-1} for **L-1**.

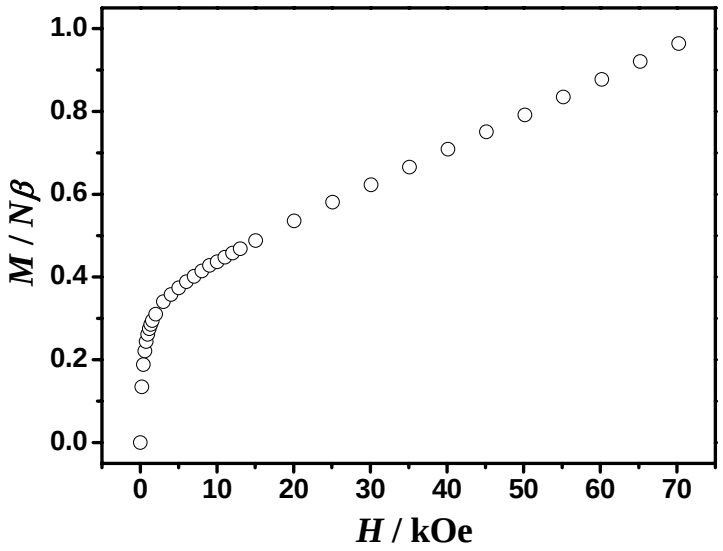

Figure S13. Plot of M vs. H for **D-1** at 2.0 K.

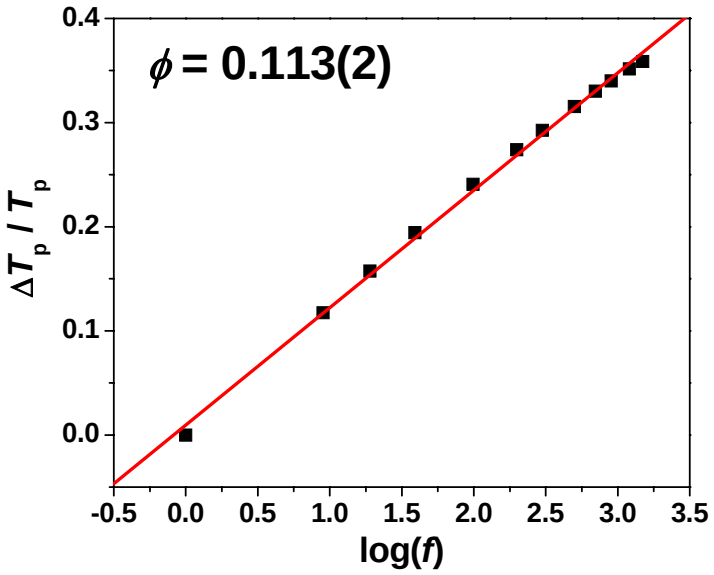

Figure S14. The log(*f*) vs. $\Delta T_p/T_p$ plot for **D-1**. The value of φ can be extracted from the slope.

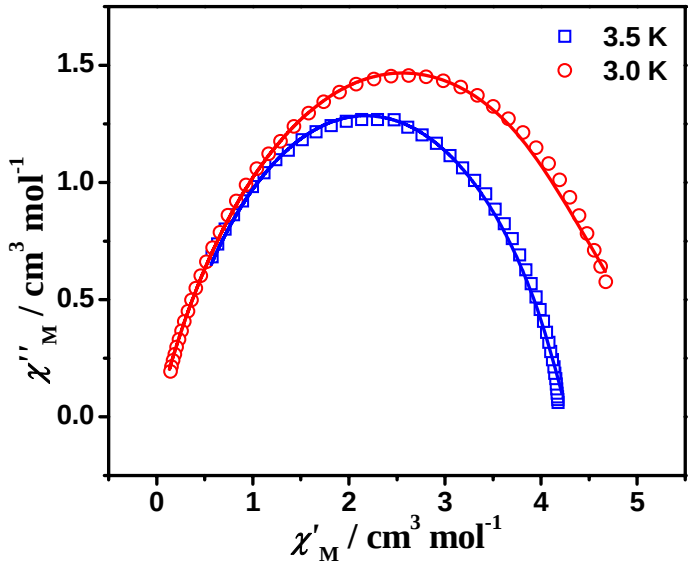

Figure S15. Cole-Cole plots for **D-1**, obtained from variable-frequency ac susceptibility data under a zero dc field at 3.0K and 3.5 K. Solid lines represent fits to the data using a generalized Debye model. The α parameters were extracted, giving 0.30-0.34.